17th World Conference on Earthquake Engineering, 17WCEE
Sendai, Japan - September 13th to 18th 2020

SPECTRAL DAMPING SCALING FACTORS FOR SUBDUCTION EARTHQUAKES

S. Rezaeian[1], Y. Bozorgnia[2], S. Mazzoni[3], L. Al Atik[4], N. Abrahamson[5], N. Kuehn[6], K. Withers[7], K. Campbell[8]

[1] *Research Structural Engineer, U.S. Geological Survey (USGS), srezaeian@usgs.gov*
[2] *Professor, University of California Los Angeles (UCLA), yousef.bozorgnia@ucla.edu*
[3] *Project Scientist, University of California Los Angeles (UCLA), smazzoni@ucla.edu*
[4] *Consultant, Linda Alatik Consulting, linda.alatik@gmail.com*
[5] *Adjunct Professor, University of California Berkeley, abrahamson@berkeley.edu*
[6] *Researcher, University of California Los Angeles (UCLA), kuehn@ucla.edu*
[7] *Research Geophysicist, U.S. Geological Survey (USGS), kwithers@usgs.gov*
[8] *Principle, Science & Analytics, CoreLogic Inc., kcampbell@corelogic.com*

Abstract

This paper presents two magnitude-distance-dependent global damping models for interface and intraslab subduction earthquakes. The Next Generation Attenuation for subduction earthquakes (NGA-Sub) project has recently developed a comprehensive database of recorded ground motions from seven subduction regions: Alaska, Cascadia, Central America and Mexico, South America, Japan, Taiwan, and New Zealand. This database is the largest uniformly processed ground motion database for subduction events and is used to develop a new set of subduction ground motion models (GMMs) at 5% damping ratio. We worked with the NGA-Sub project to develop an extended database that includes pseudo-spectral accelerations (PSA) for 11 damping ratios between 0.5 and 30%, as well as measures of significant duration of motion for each record. We use this database to develop a damping scaling factor (DSF) model that can be used to adjust subduction GMMs from a referenced 5% damping ratio to other damping ratios. The DSF is strongly influenced by the response spectrum shape and the duration of motion. Previously, as part of the "NGA-West2" project, we had developed a DSF model for shallow crustal earthquakes in active tectonic regions, which was a function of the damping ratio and spectral period, as well as magnitude and distance, which were used as surrogates for spectral shape and duration of motion. In this paper, two global DSF models are developed for the horizontal component of PSA ("RotD50" component), one for interface and one for intraslab subduction earthquakes. The parameters and functional forms for the median and standard deviation of DSF are the same as the "NGA-West2" DSF model, but the coefficients are calibrated to the NGA-Sub database. Comparisons between subduction and crustal DSF models are presented. The differences arise from the considerably longer duration of interface records for very large magnitude events and the rich high-frequency content of intraslab records compared to the shallow crustal earthquakes. Regional differences are discussed by comparing the proposed global models to the data from each subduction region, and recommendations on the applicability of the global models are provided. These models can be used to scale any subduction zone GMM for a damping ratio of 5%, including the newly developed NGA-Sub GMMs, to calculate ground motions for damping ratios other than 5%.

Keywords: Ground Motion Prediction Equations / Ground Motion Models (GMPEs/GMMs), Damping Scaling Factor (DSF), Subduction Earthquakes, Next Generation Attenuation for Subduction Earthquake (NGA-Sub)

17th World Conference on Earthquake Engineering, 17WCEE
Sendai, Japan - September 13th to 18th 2020

1. Introduction

In seismic design, analysis, and hazard calculations of engineered facilities, ground motion models (GMMs), formerly referred to as ground motion prediction equations (GMPEs), are used to predict the intensity of ground shaking. Traditionally, these GMMs are developed for the elastic pseudo-spectral acceleration (PSA) at a 5% reference damping ratio. The damping ratio represents the level of energy dissipation in structural, geotechnical, and non-structural systems. In reality, structures can have damping ratios other than 5%, depending on the structural type, construction material, and the level of ground shaking. For example, base-isolated structures typically have damping ratios much higher than 5%, while flexible tall buildings can have damping ratios as low as 2.5% [1]. The typical engineering practice is to scale the predicted 5% damped ground motion intensities ($PSA_{5\%}$) using damping scaling factors (DSFs) as shown in Eq. (1), where β represents an alternative damping ratio. A review of existing DSF models, dating all the way to the classic work of Newmark and Hall [2], can be found in Rezaeian et al. [3].

$$DSF = \frac{PSA_{\beta\%}}{PSA_{5\%}} \tag{1}$$

The majority of available DSF models are functions of the damping ratio and spectral period. Some models have recognized the importance of the duration of motion on energy dissipation (and hence on DSF) and have included other parameters as surrogates for the duration of motion in their formulations because duration of motion is not a practical parameter that is readily available to a design engineer.

1.1 DSF for Shallow Crustal Earthquakes

In the "NGA-West2" project [4, 5], we developed a parametric DSF model for shallow crustal earthquakes in active tectonic regions. This model was developed for both horizontal (i.e., RotD50 and GMRotI50) and vertical components of ground motion. In addition to damping ratio and spectral period, moment magnitude and distance were used as predictor variables to capture the effects of the duration of motion on the DSF. The functional forms for the median DSF and for its logarithmic standard deviation are shown in Eq. (2) and Eq. (3), respectively. In these equations, **M** represents the moment magnitude of earthquake and R_{rup} represents the closest distance to rupture in kilometers. The coefficients b_i, $i = 0, \dots, 8$, and a_i, $i = 1, 2$, are period-dependent and are determined empirically using a step-by-step regression process described in Rezaeian et al. [3]. For "NGA-West2", this model was fitted to over 2,000 recordings from shallow crustal earthquakes and it was concluded to be applicable for periods ranging between 0.01 and 10 s, damping ratios from 0.5 to 30%, moment magnitudes between 4.5 and 8.0, and distances less than 300 km.

$$\begin{aligned} \ln(DSF) = {} & b_0 + b_1 \ln(\beta) + b_2 (\ln(\beta))^2 \\ & + [b_3 + b_4 \ln(\beta) + b_5 (\ln(\beta))^2]\mathbf{M} \\ & + [b_6 + b_7 \ln(\beta) + b_8 (\ln(\beta))^2] \ln(R_{rup} + 1) \end{aligned} \tag{2}$$

$$\sigma_{\ln(DSF)} = \left| a_0 \ln\left(\frac{\beta}{5}\right) + a_1 \left(\ln\left(\frac{\beta}{5}\right)\right)^2 \right| \tag{3}$$

The majority of existing DSF models are developed for crustal earthquakes, where data are abundant. Very few models such as Daneshvar et al. [6] exist that focus on subduction earthquakes and discuss the differences with crustal models. In this paper, we develop two magnitude-distance-dependent global DSF models that are specific to interface and intraslab subduction earthquakes for the horizontal component (RotD50, a direction-independent measure of the two horizontal components) of ground motion.

1.2 DSF for Subduction Earthquakes

The Next Generation Attenuation for subduction earthquakes (NGA-Sub) project [7] has recently developed a comprehensive database of recorded ground motions for subduction zone earthquakes to be used in the development of a new set of subduction GMMs for 5% damping ratio. This database of over 70,000 recordings is the largest uniformly processed ground motion database for subduction events to date and includes data from seven regions. We worked with the NGA-Sub project to develop an extended database that includes PSA for 11 different damping ratios: 0.5, 1, 2, 3, 5, 7, 10, 15, 20, 25, and 30%, as well as measures of significant duration of motion (based on various levels of Arias intensity) for each record. In this paper, we use this database to empirically develop global subduction DSF models.

In 2018, a preliminary analysis of a subset of the NGA-Sub data [8], revealed that the shape of the crustal DSF model in Eq. (2) can fairly capture the overall behavior of the subduction DSF data with respect to spectral period, damping ratio, duration, magnitude, and distance, for almost all regions included in the NGA-Sub database. The largest discrepancies between the subduction data and the crustal DSF model were seen for very small and very large magnitudes (below 5 and above 8), and for small distances less than 100 km (particularly at periods greater than about 1 s), as well as for large distances greater than 300 km (particularly at periods shorter than about 0.5 s), i.e., outside the applicable range of the crustal model or where the subduction data are very limited. Overall, a more significant dependency of subduction DSF on spectral period was observed compared to crustal DSF, suggesting that the regression coefficients should be recalibrated to better fit subduction data. Furthermore, the subduction DSF data showed more dependencies on site parameters (e.g., shear-wave velocity of the top 30 m in soil, V_{S30}, and basin depth terms, Z_1 and $Z_{2.5}$) compared to the crustal data. Note that these site parameters were not included in Eq. (2) because they were not very influential on crustal DSF [4, 5]. Finally, systematic differences were seen between the DSF for subduction interface and subduction intraslab earthquakes.

Based on the conclusions from Rezaeian et al. [8], the proposed model in this paper retains the functional forms in Eq. (2) and Eq. (3), but recalibrates the period-dependent regression coefficients $b_0, \dots, b_8$ and a_0 & a_1 to achieve a better fit to the NGA-Sub data. Furthermore, two magnitude-distance-dependent global DSF models (i.e., two sets of regression coefficients) are developed separately for the interface and for the intraslab subduction earthquakes. Finally, a discussion is provided on possible future updates of the model by including additional predictor variables that represent site parameters.

2. NGA-Sub DSF Database

The NGA-Sub database for $PSA_{5\%}$ contains over 70,000 recordings from over 900 earthquakes from seven regions: Alaska (ALK), Cascadia (CAS), Central America and Mexico (CAM), South America (SAM), Japan (JPN), Taiwan (TWN), and New Zealand (NZL). For developing a DSF model, we calculated the horizontal PSA (i.e., RotD50 component) at all 11 damping ratios listed above for events that have a moment magnitude of $\mathbf{M} \geq 4.5$ and a distance of $R_{rup} \leq 1000$ km (the range of interest for modeling). This reduced our database to 59,170 recordings from 926 earthquakes. We then only selected the data from subduction interface events (i.e., "Intra_Inter_Flag" equal to 0) and subduction intraslab events (i.e., "Intra_Inter_Flag" equal to 1 or 5), excluding the shallow crustal/overriding events and outer rise events as well as interface and intraslab subduction events with small confidence, based on the categorization by NGA-Sub project [7]. This resulted in two separate databases of over 19,000 recordings from over 300 subduction interface events, and over 20,000 recordings from about 300 subduction intraslab events.

2.1 Interface Versus Intraslab

Separating the data into interface and intraslab earthquakes is important in order to capture the systematic differences between the DSFs of these two tectonic regimes. Furthermore, having two separate models helps with the application of the DSF to GMMs, which are also developed separately for interface and intraslab earthquakes. To demonstrate the differences between DSF for interface and intraslab earthquakes, Fig. 1 shows the dependency of median DSF (i.e., mean of ln(DSF), assuming a lognormal distribution for DSF) on spectral periods at all 11 damping ratios for an example magnitude-distance bin (magnitudes between 6 and 7, and distances smaller than 100 km) of data from Japan. The two subplots in this figure correspond to interface and intraslab subduction events. Both bins have comparable number of recordings (401 versus 350), as well as similar magnitudes and distances, but there is an obvious difference between the DSF of the two tectonic regimes: the peaks of the DSF of intraslab events are more extreme and happen at shorter periods with DSF approaching unity faster over period (see 1 to 10 s) compared to interface events. This behavior seems typical for all other regions and magnitude-distance bins, where data are available, supporting the decision to develop two separate models for interface and intraslab events. The dashed lines in Fig. 1 correspond to the "NGA-West2" crustal DSF model calculated at the median values of magnitude and distance for the data in each bin. These dashed lines are superimposed for comparison, showing that the crustal model has a similar shape to the subduction data but does not fit very well especially at longer periods beyond 1 s and particularly for intraslab records in the case of Japan. This supports our decision that the regression coefficients in Eq. (2) should be calibrated to subduction-specific data.

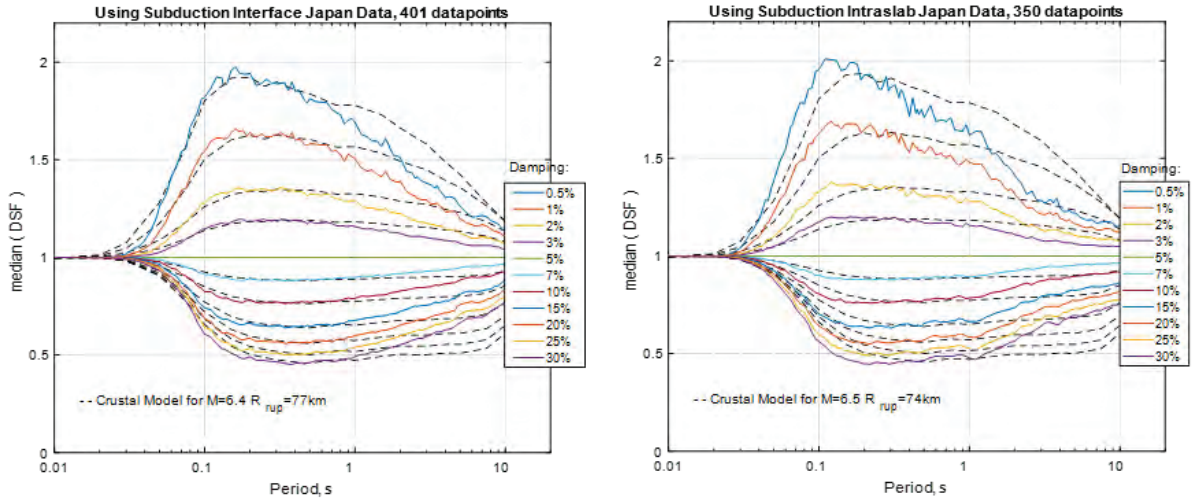

Fig. 1 – Differences between subduction interface and intraslab DSF. The solid lines show the median DSF from Japan recordings with magnitudes between 6 and 7, and with distances less than 100 km. The dashed lines show the crustal DSF model for the corresponding mean magnitude and distance.

2.2 Selected Records for Modeling

To ensure that only data with good quality are used in modeling (i.e., in regression), we further reduce the number of recordings in our database by only selecting the records that were also used by two of the NGA-Sub GMM developer teams. Each team independently evaluated the NGA-Sub data based on their own individual selection criteria (one team selected a total of about 16,000 records; while the other selected only 7,000 records). They both discarded recordings beyond the distance R_{max}, which is a new parameter provided in the NGA-Sub database that considers the triggering threshold of the recording instruments. We

discarded any recordings that were not selected by at least one of the two developer teams, reducing our database to about 7,000 recordings for interface events and to about 9,000 recordings for intraslab events, which are still very large numbers for model development. The magnitude-distance distribution of this "GMM-selected" database is shown in Fig. 2.

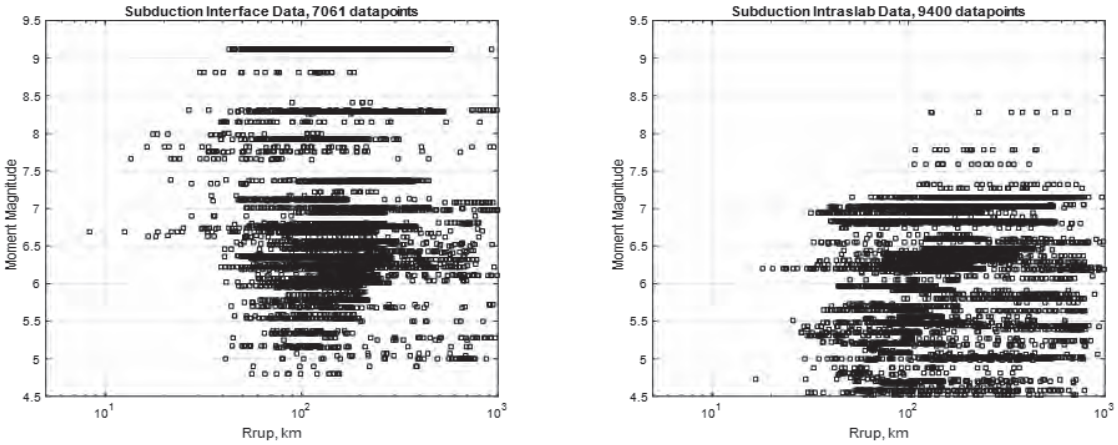

Fig. 2 – Magnitude-distance distribution of selected records from subduction interface (left) and subduction intraslab (right) earthquakes.

Compared to the "NGA-West2" database for shallow crustal earthquakes [4], magnitudes of subduction events are generally larger, especially for interface subduction events, and data for shorter distances are sparse (below 50 km). In the development of the crustal DSF model [4], we only used the data with $R_{rup} \leq 50$ km to derive the regression coefficients and then extended the applicability of our model to 300 km by checking residuals between 50 and 300 km. For subduction events, we have a very limited number of recordings below 50 km, but a relatively good collection below 100 km, from 100 to 300 km and 300 to 1000 km. Therefore, we use these three distance bins for scrutinizing our data. Since subduction ground motions are generally stronger at a given distance and are felt at longer distances compared to crustal ground motions, we will develop our subduction DSF model for distances up to 1000 km, paying special attention to data for distances below 300 km, where a lot of data are available and ground motions are relatively larger and hence more capable of inflicting damage.

The statistics of the selected records are summarized and broken down by regions in Tables 1 and 2 for interface and intraslab subduction earthquakes, respectively. These tables show the three-letter abbreviation for each of the seven regions, the number of recordings from each region, ranges of moment magnitude **M**, distance R_{rup}, duration D_{5-75} (time from 5% to 75% levels of Arias intensity), site parameter V_{S30}, and basin depth terms Z_1 and $Z_{2.5}$. The last two columns $\rho_{D,M}$ and $\rho_{D,R}$ show the linear correlation coefficients between the duration of motion and magnitude, and the duration of motion and distance, respectively. The same data for all regions (i.e., global data) are shown in the last row of each table. As expected, very few interface recordings are available from ALK and CAS regions, but the contribution from these regions increases for intraslab recordings.

The global dataset for interface earthquakes has a good representation of magnitudes with a mean of 7.08, distances with a mean of 189 km, duration with a mean of 46 s, and site parameters V_{S30}, Z_1 and $Z_{2.5}$ (means of 447 m/s, 170 m, and 780 m, respectively). The correlations $\rho_{D,M}$ and $\rho_{D,R}$ are relatively high (0.69 and 0.60) as expected on the global scale, but they vary from region to region. Duration seems to

consistently be highly correlated with distance in all regions, but the high correlation with magnitude seems to be more in line with data from Japan and New Zealand.

The global dataset for intraslab earthquakes also has a good representation of magnitudes (generally smaller than interface, as expected) with a mean of 6.16, distances with a mean of 207 km, duration with a mean of 34 s (generally shorter than interface, as expected), and site parameters V_{S30}, Z_1, and $Z_{2.5}$ (means of 467 m/s, 179 m, and 792 m, respectively). The correlation $\rho_{D,R}$ (0.76) is higher than $\rho_{D,M}$ (0.46) on the global scale, as well as for each region.

Table 1 – Interface Subduction Earthquake Recordings (selected data used in modeling)

Region	Number of Records	M	R_{rup} (km)	D_{5-75} (s)	V_{S30} (m/s)	$Z_{1.0}$ (m)	$Z_{2.5}$ (m)	$\rho_{D,M}$	$\rho_{D,R}$
ALK	204	[5.0, 7.0]	[45, 968]	[7, 374]	[322, 750]	-	-	-0.12	0.85
CAS	8	4.9	[57, 387]	[5, 103]	[455, 665]	-	[0, 1289]	0	0.98
CAM	99	[6.3, 7.99]	[14, 780]	[5, 212]	[225, 586]	-	-	-0.70	0.92
SAM	733	[6.1, 8.81]	[16, 995]	[5, 444]	[198, 1951]	-	-	0	0.78
JPN	5,427	[4.8, 9.12]	[8, 929]	[3, 456]	[94, 2230]	[0, 2194]	[0, 5234]	0.69	0.61
TWN	549	[5.68, 7.12]	[48, 679]	[7, 208]	[121, 1402]	[0, 1154]	[34, 1080]	-0.33	0.83
NZL	41	[5.0, 7.81]	[35, 199]	[11, 69]	[210, 1500]	[0, 300]	-	0.42	0.44
All Regions:	7,061	[4.8, 9.12]	[8, 995]	[3, 456]	[95, 2230]	[0, 2194]	[0, 5234]	0.69	0.60

Table 2 – Intraslab Subduction Earthquake Recordings (selected data used in modeling)

Region	Number of Records	M	R_{rup} (km)	D_{5-75} (s)	V_{S30} (m/s)	$Z_{1.0}$ (m)	$Z_{2.5}$ (m)	$\rho_{D,M}$	$\rho_{D,R}$
ALK	648	[5.0, 7.15]	[77, 963]	[7, 219]	[243, 750]	-	-	-0.03	0.79
CAS	589	[4.52, 6.8]	[26, 940]	[1, 377]	[131, 1522]	-	[0, 6831]	0.21	0.91
CAM	52	[6.26, 7.32]	[47, 713]	[7, 155]	[281, 2100]	-	-	0.42	0.73
SAM	350	[6.07, 7.78]	[46, 989]	[7, 173]	[116, 1639]	-	-	-0.27	0.78
JPN	3,904	[4.75, 8.28]	[18, 648]	[2, 155]	[95, 2100]	[0, 2129]	[0, 4169]	0.48	0.78
TWN	3,477	[4.56, 7.02]	[32, 694]	[1, 183]	[121, 1538]	[0, 1154]	[34, 1080]	0.28	0.80
NZL	380	[4.55, 6.65]	[17, 285]	[2, 97]	[120, 1200]	[0, 1000]	-	0.39	0.59
All Regions:	9,400	[4.52, 8.28]	[17, 989]	[1, 377]	[95, 2100]	[0, 2129]	[0, 6830]	0.46	0.76

3. Model Development

To make a model for the median DSF, we follow a step-by-step regression process as described in [3]. Regression is done separately at 21 spectral periods: $T = 0.01$, 0.02, 0.03, 0.05, 0.075, 0.1, 0.15, 0.2, 0.25, 0.3, 0.4, 0.5, 0.75, 1, 1.5, 2, 3, 4, 5, 7.5, and 10 s. To ensure that the best quality data are used in our regression, we only use the PSA data above the shortest and below the longest usable periods (these periods are reported in the NGA-Sub database and were calculated based on the filters used in the processing of each record) to calculate the DSF in Eq. (1). As a result, fewer data points are utilized in the regressions at

shorter and longer spectral periods compared to the total number of data points mentioned in the previous section.

We start by including both parameters **M** and R_{rup} in the model, as surrogates for the duration of motion, and perform regression at every combination of the 11 damping ratios and the 21 spectral periods, using the simple functional form shown in Eq. (4).

$$\ln(DSF) = c_0 + c_1\mathbf{M} + c_2 \ln(R_{rup} + 1) \tag{4}$$

At every step, we observe that the coefficients of the constant term c_0, the magnitude term c_1, and the distance term c_2, are obvious functions of the damping ratio that can be fitted with a quadratic function of $\ln(\beta)$, leading to the functional form in Eq. (2). Fig. 3 demonstrates the dependency of these coefficients on the damping ratio at an example period of 1 s for subduction interface recordings. The behavior of c_0, c_1, and c_2, changes between a linear function of $\ln(\beta)$, e.g., Fig. 3c, to a quadratic function of $\ln(\beta)$, e.g., Fig. 3a, depending on the spectral period. A quadratic function, however, can fit all three coefficients at all periods well and is shown in the examples of Fig. 3 as the "fitted" lines. It also provides a consistent functional form with the crustal model in Eq. (2).

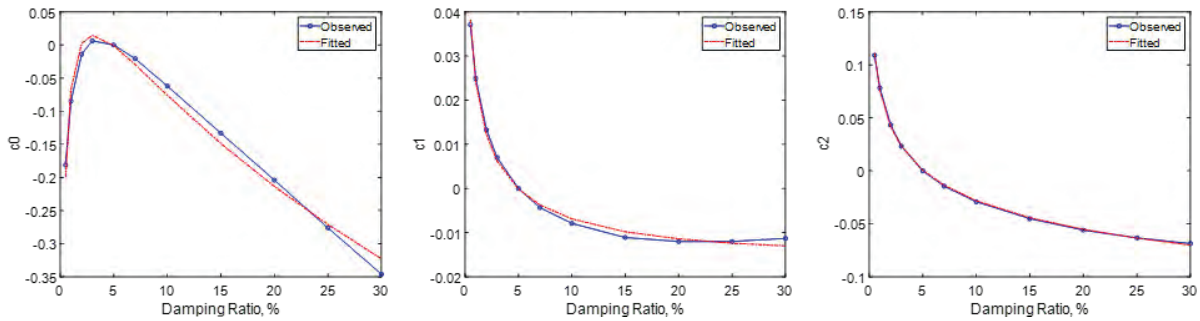

(a) (b) (c)

Fig. 3 – Coefficients of (a) the constant term c_0, (b) the magnitude term c_1, and (c) the distance term c_2, as functions of the damping ratio for a spectral period of 1 s for subduction interface recordings.

3.1 Period-Dependent Coefficients

The regression coefficients b_0, …, b_8 from Eq. (2) are determined from the fitted functions to c_0, c_1, and c_2 (e.g., red "fitted" lines in Fig. 3) at every given spectral period. These coefficients are plotted in Fig. 4 as functions of periods or both interface and intraslab subduction earthquakes. The coefficients of the crustal DSF model from "NGA-West2" are also shown in this figure for comparison. Note that the scales are different for each coefficient to allow better visual representation, but they are proportional. For example, the scales of the y-axis for coefficients b_0, b_3, and b_6 (i.e., coefficients of terms independent of β) are twice as large as the scales for coefficients b_1, b_4, and b_7 (i.e., coefficients of terms with $\ln(\beta)$), and those are twice as large as the scales for coefficients b_2, b_5, and b_8 (i.e., coefficients of terms with $\ln(\beta)^2$). This gives us a sense of the relative importance of each term in Eq. (2). From this figure, we can see that the coefficients of the constant term and the magnitude term are more different from those of the crustal earthquakes for subduction interface events compared to intraslab events. On the other hand, coefficients of the distance term for subduction intraslab events show more deviation from their crustal counterparts at longer periods.

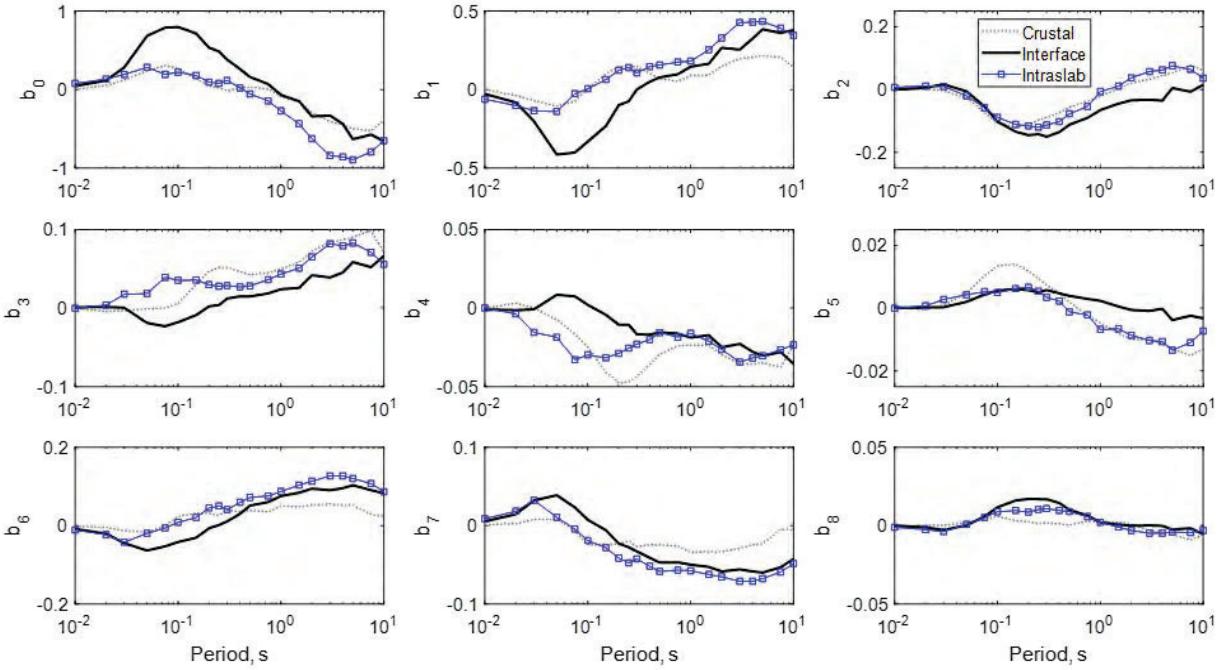

Fig. 4 – Period-dependent coefficients in Eq. (2) for subduction interface, subduction intraslab, and crustal earthquakes for horizontal RoD50 component of ground motion.

3.2 Standard Deviation

To make a model for the standard deviation of ln (DSF), we calculate the residuals between the right side and the left side of Eq. (2). After checking that the mean is zero, the sample dispersions are used to estimate the standard deviation at every spectral period and damping ratio under consideration. These standard deviations (i.e., "observed") are shown in Fig. 5 at four example periods $T = 0.1, 0.2, 1,$ and 7.5 s for the subduction interface events. Note that the standard deviation at 5% damping ratio is 0 (since the scaling factor is equal to 1 without uncertainty) and it increases as the damping ratio deviates from 5%.

To model the standard deviation, we consider two functions of the damping ratio: (a) a linear function of ln (β), i.e., $a_1 = 0$ in Eq. (3), and (b) a quadratic function of ln (β), i.e., using Eq. (3). These two alternative functions (i.e., "fitted") are also shown in Fig. 5. Note that the fit of the simpler function with only a_0 as the coefficient is not too bad and in fact is very good at some periods such as 1 s, but the fit of the function in Eq. (3) is much better and it works at all periods. Because of this, we recommend the use of Eq. (3) as was done for crustal earthquakes to achieve more accuracy in our model. Although not shown in Fig. 5, the same behavior and conclusions hold for subduction intraslab events.

Finally, Fig. 6 plots the two coefficients of the standard deviation, a_0 and a_1, as functions of periods for both subduction interface and intraslab events. It further compares them to their counterparts from the "NGA-West2" crustal model. Overall, the differences between the different models are not significant, with the exception that the subduction events show larger standard deviations at shorter periods around 0.1 s (absolute values of a_0 are larger for subduction compared to crustal events).

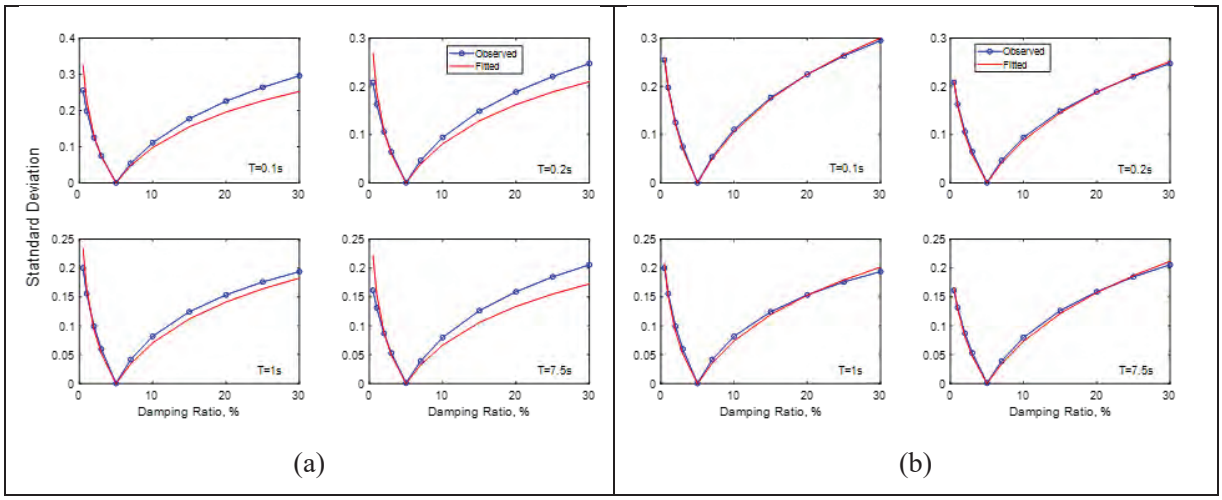

Fig. 5 – Standard deviations of ln (DSF) at four example periods 0.1, 0.2, 1, and 7.5 s for interface subduction events. "Observed" lines are the same in (a) and (b). "Fitted" lines are different: (a) linear functions of ln (β), i.e., $a_1 = 0$ in Eq. (3), and (b) quadratic functions of ln (β), i.e., Eq. (3).

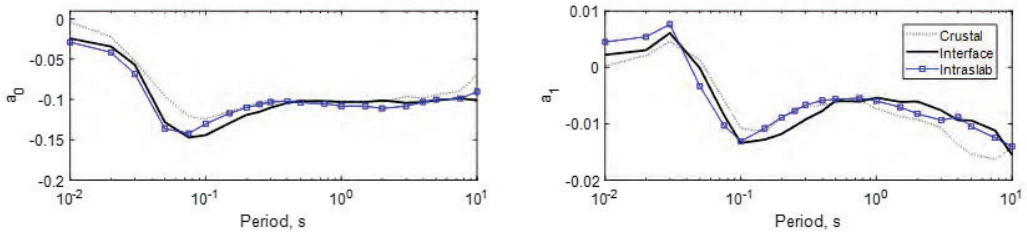

Fig. 6 – Period-dependent standard deviation coefficients a_0 (left) and a_1 (right).

3.3 Residuals with Magnitude, Distance, and Duration

We know that the duration of motion is an important parameter that influences the DSF; however, explicit inclusion of duration in the model is not ideal in practice because duration is generally not available to a design engineer. In general, duration is controlled by the earthquake magnitude and distance from the rupture. Therefore, we hope that the inclusion of magnitude and distance in the model takes care of the dependencies on the duration of motion. After performing regression using Eq. (2) and scrutinizing the residual diagnostic plots, we find that most of the influence of duration on DSF can in fact be captured through inclusion of **M** and R_{rup} in the model. The residuals versus **M**, R_{rup}, and D_{5-75} are examined at every combination of the 11 damping ratios and 21 spectral periods. In general, a linear magnitude term is necessary and sufficient to capture the dependencies of residuals on **M**, and it also reduces the dependencies on the duration of motion. A logarithmic function of R_{rup} captures the dependencies of residuals on distance and further reduces the dependencies on D_{5-75}. Examples of residual plots versus **M**, R_{rup}, and D_{5-75}, are shown in Fig. 7 at a damping ratio of 20% and a period of 1 s. The black lines in this figure are crude representations of mean residual patterns. We can see that the residuals are symmetrically scattered above and below the zero level with no obvious systematic trends with respect to **M** and R_{rup}. Also, we can observe that most of the pattern with D_{5-75} has been resolved even though duration is not an explicit

parameter in the model. A slight remaining trend (possibly quadratic) in the residuals versus duration suggests that other parameters (perhaps site or basin parameters) should be added to the model to further improve the residuals with the duration of motion.

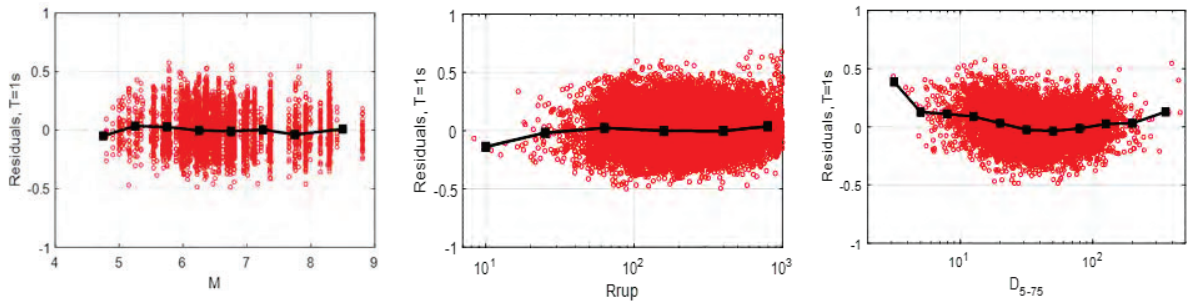

Fig. 7 – Example residual plots for subduction interface DSF model at 20% damping and 1 s period.

4. The Proposed M-R-Dependent Global Subduction DSF Models

We calculate the proposed magnitude-distance-dependent global subduction DSF models according to Eq. (2) and the regression coefficients shown in Fig. 4 at two example magnitudes of 7 and 8 and at two distances of 100 and 300 km. The resulting estimates of median DSF are shown in Fig. 8 for both interface and intraslab earthquakes. In this figure, the crustal DSF is also shown for comparison. In general, the peak of median *DSF* for the intraslab earthquakes is shifted towards shorter periods and is more extreme, suggesting higher frequency contents. Also, the most significant differences between subduction and crustal events are seen at longer periods and larger damping ratios, where the subduction DSF approaches unity faster; this difference is greater at larger magnitudes and distances where the crustal model was an obvious extrapolation, and hence not expected to behave well.

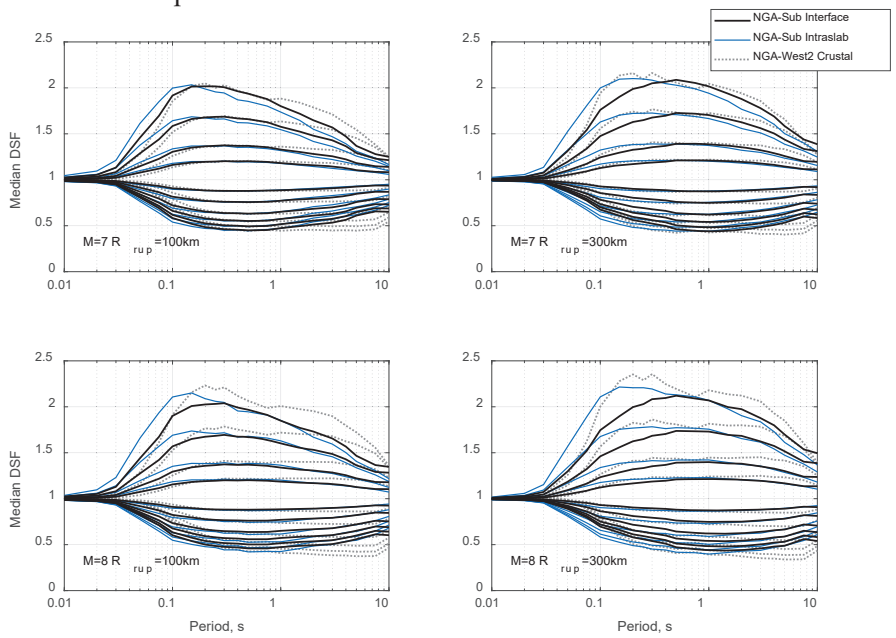

Fig. 8 – The proposed global subduction models for median DSF of interface and intraslab earthquakes. The crustal model from "NGA-West2" (gray dotted lines) is superimposed for comparison.

4.1 Comparisons of the Proposed Global Models to the Region-Specific Data

We compare the global subduction models of median DSF (proposed in previous sections) to the data from each of the seven subduction regions. This helps us to assess the applicability of the proposed global models for each specific region. Of course, the challenge is that the data from some regions are very limited, for example, Alaska (ALK) and Cascadia (CAS) regions do not have enough large magnitude data for interface earthquakes (see Tables 1 and 2). Therefore, the use of a global model is recommended in the absence of data in such regions. Examples of such comparisons for Alaska and Japan are shown in Fig. 9 and Fig. 10, respectively.

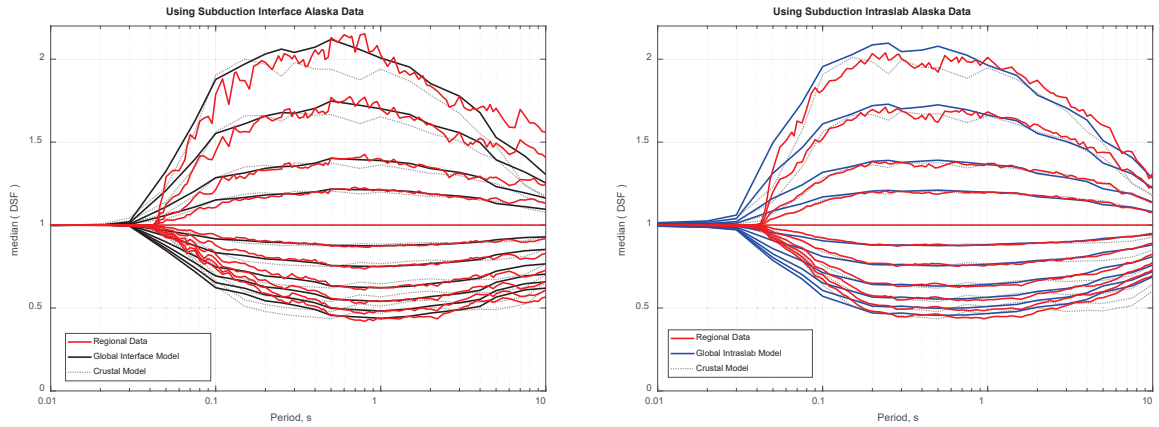

Fig. 9 – Alaska data versus global models.

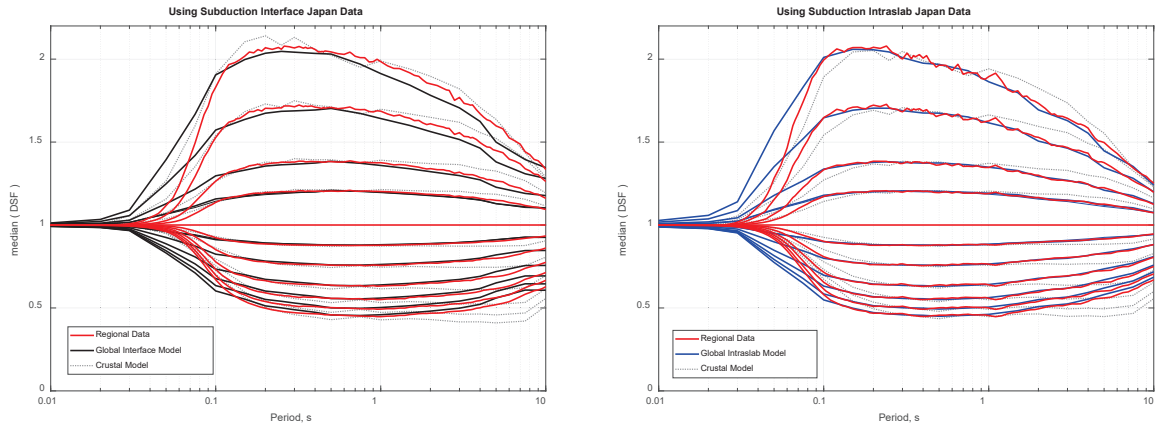

Fig. 10 – Japan data versus global models.

The models in Fig. 9 and Fig. 10 are calculated and plotted for magnitude and distances equal to the mean values of magnitude and distance for the selected set of regional data (i.e., **M**=5.7 and R_{rup} = 451 km for Alaska interface, **M**=5.8 and R_{rup} = 439 km for Alaska intraslab; **M**=7.2 and R_{rup} = 174 km for Japan interface, **M**=6.6 and R_{rup} = 211 km for Japan intraslab). The global subduction models fit the data better than the existing crustal model, which is also shown in these figures for comparison, and therefore are recommended for periods longer than 0.1 s in all subduction regions. At shorter periods, below

0.1 s (which are not typical of most practical structures), the models may require improvement by including other parameters that better capture high-frequency content of the ground motion and are not recommended.

5. Conclusion and Future Direction

This paper develops and presents magnitude-distance-dependent global subduction models for the damping scaling factors (DSFs) of interface and intraslab earthquakes for the horizontal (RotD50) component of ground motion. The functional forms for the median DSF and its standard deviation are the same as those for the crustal "NGA-West2" DSF model, but the coefficients are different and derived using the newly developed "NGA-Sub" database for subduction earthquakes from seven regions. The proposed models can be used to scale subduction-specific GMMs (including NGA-Sub GMMs) from a 5% damping ratio to other damping ratios from 0.5 to 30%. They are applicable to magnitudes between 4.5 and 9, and to distances up to 1000 km. The models are recommended for periods from 0.1 s to 10 s. For periods shorter than 0.1 s and for improved residual patterns with the duration of motion, future revisions of the model could consider adding variables that better describe high-frequency content, site terms, or basin depths.

6. Acknowledgement

This research was partially supported by the U.S. Geological Survey (USGS). The development of the NGA-Sub database was partially supported by FM Global and the USGS. These supports and the constructive interactions with the NGA-Sub researchers through numerous meetings are gratefully acknowledged. The opinions and findings are those of the authors, supported by the USGS, but do not necessarily reflect the views of all sponsoring agencies.

7. References

[1] TBI: Tall Buildings Initiative (2010): Guidelines for performance-based seismic design of tall buildings. *Technical Report PEER 2010/05*. Prepared by the TBI Guidelines Working Group. Berkeley, California: Pacific Earthquake Engineering Research Center, University of California.

[2] Newmark NM, Hall WJ (1982): Earthquake spectra and design. *Technical Report,* Earthquake Engineering Research Institute, Berkeley, CA.

[3] Rezaeian S, Bozorgnia Y, Idriss IM, Campbell K, Abrahamson N, Silva W (2012): Spectral damping scaling factors for shallow crustal earthquakes in active tectonic regions. *Technical Report PEER 2012/01*, Pacific Earthquake Engineering Research, Berkeley, CA.

[4] Rezaeian S, Bozorgnia Y, Idriss IM, Abrahamson N, Campbell K, Silva W (2014): Damping scaling factors for elastic response spectra for shallow crustal earthquakes in active tectonic regions: "average" horizontal component. *Earthquake Spectra,* **30** (2): 939-963.

[5] Rezaeian S, Bozorgnia Y, Idriss IM, Abrahamson N, Campbell K, Silva W (2014): Damping scaling factors for vertical elastic response spectra for shallow crustal earthquakes in active tectonic regions. *Earthquake Spectra,* **30** (3): 1335-1358.

[6] Daneshvar P, Bouaanani N, Goda K, Atkinson GM (2016): Damping reduction factors for crustal, inslab, and interface earthquakes characterizing seismic hazard in southwestern British Columbia, Canada. *Earthquake Spectra*, **32** (1), 45–74. https://doi.org/10.1193/061414EQS086M.

[7] Bozorgnia Y, Kishida T, Abrahamson N, Ahdi S, Ancheta T, Archuleta R, Atkinson G, Boore D, Campbell K, Chiou B, Contreras V, Darragh R, Gregor N, Gulerce Z, Idriss IM, Ji C, Kamai R, Kuehn N, Kwak D, Kwok A, Lin P, Magistrale H, Mazzoni S, Muin S, Midorikawa S, Parker G, Si H, Silva W, Stewart J, Walling M, Wooddell K, Youngs R (2018): NGA-subduction research program. *Proceedings of the 11th U.S. National Conference on Earthquake Engineering (11NCEE)*, Los Angeles, CA, June 25-29, paper 1705.

[8] Rezaeian S, Bozorgnia Y, Kishida T (2018): Spectral damping scaling factors for subduction interface and intraslab earthquakes. *Proceedings of the 11th U.S. National Conference on Earthquake Engineering (11NCEE)*, Los Angeles, CA, June 25-29, paper 751, 11 p.

